Signal Processing 231 (2025) 109898

Contents lists available at ScienceDirect

Signal Processing

journal homepage: www.elsevier.com/locate/sigpro

Single atom convolutional matching pursuit: Theoretical framework and application to Lamb waves based structural health monitoring

Sebastian Rodriguez [a,*], Marc Rébillat [a], Shweta Paunikar [a], Pierre Margerit [a], Eric Monteiro [a], Francisco Chinesta [a,b], Nazih Mechbal [a]

[a] PIMM, Arts et Métiers ParisTech, CNRS, CNAM, 151 Boulevard de l'Hôpital, Paris, 75013, France
[b] CNRS@CREATE LTD, 1 Create Way, #08-01 CREATE Tower, Singapore, 138602, Singapore

ARTICLE INFO

Keywords:
Lamb waves
Convolutional matching pursuit
Matching pursuit
Structural health monitoring
Single atom dictionary

ABSTRACT

Lamb Waves (LW) based Structural Health Monitoring (SHM) aims to monitor the health state of thin structures. An Initial Wave Packet (IWP) is sent in the structure and interacts with boundaries, discontinuities, and with eventual damages thus generating many wave packets. An issue with LW based SHM is that at least two LW dispersive modes simultaneously exist. Matching Pursuit Method (MPM), which approximates a signal as a sum of delayed and scaled atoms taken from a known dictionary, is limited to nondispersive signals and relies on a priori known dictionary and is thus inappropriate for LW-based SHM. Single Atom Convolutional MPM, which addresses dispersion by decomposing a signal as delayed and dispersed atoms and limits the learning dictionary to only one atom, is alternatively proposed here. Its performances are demonstrated on numerical and experimental signals and it is used for damage monitoring. Beyond LW-based SHM, this method remains very general and applicable to a large class of signal processing problems.

1. Introduction

In industrial applications, one of the major engineering challenges is to monitor structural damage automatically, in order to prevent catastrophic failure, and this process is known as structural health monitoring (SHM) [1,2]. A classic SHM procedure generally consists of five stages [2–7]: detection, localization, classification, quantification, and prognostic. The term *"damage"* is used here to define changes in the material properties and/or geometry of these structures, including boundary conditions, which have a negative effect on its current or future performance [8].

Among the various existing SHM techniques dedicated to thin composite or metallic structures, strategies based on ultrasonic Lamb Waves (LW) emitted and received by piezoelectric elements (termed PZT[1] in the following of the manuscript) are particularly effective [1,9–11]. LW are bending and compression waves (also called A0 and S0 modes in their lower frequency range) that stress the entire thickness of the thin structure being monitored. These waves have the particularity of being able to propagate over relatively large distances and can therefore cover a large control surface with few PZTs in a short time. However, LW possesses two main drawbacks: at any given frequency, at least two modes simultaneously coexist (namely A0 and S0), and these modes are dispersive, meaning that LW velocities depends on the frequency, which makes the interpretation of the collected signals tricky in practice.

The basic idea underlying LW-based SHM is then to excite one PZT bonded on the structure to monitor with a tone burst signal centered around a given frequency. This Initial Wave Packet (IWP) then propagates through the structure to be inspected and interacts with its boundaries, its structural discontinuities, and eventual damages. Each of these discontinuities produces an additional wave packet propagating in the host structure. Consequently, the resulting signals measured by the other PZT correspond to the IWP after propagation within the host structure and multiple interactions caused by structural discontinuities. In particular, LW based SHM algorithms seek to detect echoes caused by the presence of damage in such signals in order to infer damage presence, location, type, and severity.

In such a context, being able to decompose measured signals as many wave packets that can be physically interpreted and potentially linked to structural damages is of great interest. Several signal processing methods have already been proposed to address this issue [12,13].

* Corresponding author.
E-mail address: sebastian.rodriguez_iturra@ensam.eu (S. Rodriguez).

[1] This acronym, widely used in the scientific literature originate from French as "Plomb Zirconium Titanate" (in english "Lead zirconate titanate") and describes the chemical composition of the powders that are used to build up the piezoelectric elements.

https://doi.org/10.1016/j.sigpro.2025.109898
Received 25 July 2024; Received in revised form 27 December 2024; Accepted 13 January 2025
Available online 18 January 2025
0165-1684/

Among the existing methods, Matching Pursuit Method (MPM) [14] proposes to approximate a given signal $s(t)$ as follows:

$$s(t) \approx \sum_{i=1}^{m} \alpha_i \Psi_i(t) \tag{1}$$

The features extracted by MPM accordingly to Eq. (1) correspond to the atoms $\Psi_i(t)$ and their amplitudes α_i. Typically the atoms $\Psi_i(t)$ are selected on an over-complete learning dictionary D that needs to be provided a priori [15–19], where functions $\Psi_i(t)$ are selected in a greedy process in the sparsest way possible. However, MPM is limited only to non-dispersive signals, preventing its application in SHM for thin structures where LW undergoes dispersion during propagation. In this case, in addition to delays and attenuation, wave packets also endure dispersion caused by the fact that all the frequencies do not propagate at the same speed within the structures under study. Furthermore, the learning dictionary D needs to be a priori defined, which limits the practical use of MPM as not all delayed, attenuated, and dispersed atoms cannot be precomputed in advance for both A0 and S0 modes propagating in a continuous thin structure.

Despite these drawbacks, MPM has, however, already been applied in an LW based SHM context in combination with other methods for damage monitoring. Recently, Li et al. [20] developed a method using orthogonal matching pursuits and model updating to locate damages in hinge joints of a fully functional hollow slab bridge using data collected from a single location. To decompose and reconstruct the various wave packets in a signal, Gao et al. [21] used orthogonal matching pursuit algorithm based on dictionary matrix, while Kim and Yuan [22] used it for imaging damage in an aluminium plate, and Li et al. [23] used it to reconstruct normalized electromechanical admittance data to develop an SHM system for a concrete tunnel. Mu et al. [24] also used orthogonal MP in conjunction with dispersion removal for identifying LW packets in shells. MPM is employed by Hong et al. [25] to analyze guided wave signals obtained from FE simulations and experiments in the covered region of the metallic messenger cable in an electrified railway catenary and successfully detect damage larger than 2.5 mm in the cable. An optimized dictionary based MPM was employed to study and size axial defects in in-service or corroded pipelines by Tse and Wang [26]. It is noteworthy that all of these methods are based on predefined over-complete dictionaries for employing MPM.

In addition to dictionary based approaches [27–30], non-dictionary based approaches like Variational Mode Decomposition (VMD), Empirical Mode Decomposition (EMD), Proper Orthogonal Decomposition, etc., have also been used by researchers to decompose wave signals in different domains. Cuomo et al. [31] applied Hilbert Huang transform based EMP to decompose a multi-component signal and detect impact damage in aluminium and CFRP plates. A modified two parameters based VMD method was used by Jiang et al. [32] to identify wave modes in multi-mode ultrasonic wave signals and further detect and quantify internal holes of various sizes at various depths in rail specimens. Another version of VMD, which extracts the mode functions successively using four pre-defined decomposition criteria, is used by Zeng et al. [33] to identify faults in long electrical transmission cables. However, these non-dictionary based approaches are based on a mathematical basis and not on any physical basis, thus limiting the interpretability of the provided results in practice.

An improved version of Matching Pursuit is thus proposed in the present work. It addresses the decomposition of LW based SHM signals by decomposing a measured signal as delayed and dispersed impulse response of a single atom. This decomposition is called here the *Single Atom Convolutional Matching Pursuit Method* (SACMPM). First, a theoretical framework is presented for the computation of MPM where a purely mathematical construction of the decomposition is achieved without the need of an over-represented learning dictionary which is called here the *Single Atom Matching Pursuit Method* (SAMPM). Here, only a single atom $\Psi(t)$ is used, which is considered to be the external excitation imposed on the structure and corresponds to the Initial Wave Packet. A theoretical framework allowing to numerically obtain the optimal amplitudes and time delay of a SAMPM decomposition is presented following a *Greedy* process building the decomposition on-the-fly until convergence. Then, its extension to the SACMPM, taking into account dispersion effects through a convolution operation, is introduced on the basis of the previous theoretical framework. Both methods are afterward applied to experimental LW based SHM signals for comparison purposes and to highlight the benefits offered by the SACMPM. Finally, damage localization is achieved through the use of machine Learning algorithms fed by features extracted from SAMPM and SACMPM thus demonstrating its practical interest for SHM purposes.

It should be noted that the signal approximation methods proposed in this paper (SAMPM and SACMPM) remain completely general and can be easily applied to any signal processing problem.

The present paper is thus structured as follows: Section 2 introduces the *Single Atom Matching Pursuit Method* (SAMPM) and the proposed associated theoretical framework. Section 3 then extends it to *Single Atom Convolutional Matching Pursuit* (SACMPM). Following Section 4 and Section 5 provide numerical analysis on the performance of the proposed techniques when they approximate real signals and when they are used to predict damage location, respectively. Finally, Section 7 provides conclusions and perspectives.

2. Single atom matching pursuit method theoretical framework

The Single Atom Matching Pursuit Method (SAMPM) is introduced here along with the theoretical framework allowing to numerically build the optimal decomposition without the need for a priori known learning dictionary.

2.1. Selecting a single initial atom

For LW-based SHM applications, the excitation signal is known and corresponds to the Initial Wave Packet (IWP) being sent on the structure. This signal is usually a tone burst centered around a given central frequency, as shown in Fig. 1. As this IWP is the origin of all the upcoming echoes appearing in the host structure and being later measured, it can naturally be used as the only atom contained in the learning dictionary. The main assumption made in that case is that this single IWP is at the core of all the other generated wave packets and thus can be used as the single atom that is necessary in the learning dictionary. As the signal being sent to PZT is systematically recorded in LW-based SHM applications, this single atom is readily available in practice, and thus, there is no need for any a priori known learning dictionary in the present case.

2.2. Frequency domain greedy approach

The main idea behind SAMPM then consists in approximating a given measured signal $s(t)$ after its propagation within the structure to be inspected by the following decomposition:

$$s(t) \approx s_m(t) = \sum_{i=1}^{m} \alpha_i \Psi(t - \tau_i) \tag{2}$$

where the principal unknowns to be determined by the MPM algorithm correspond to the amplitude of each term α_i and its temporal delay τ_i and the only considered atom $\Psi(t)$ corresponds to the one that has been previously selected. It is proposed here that each term of the decomposition of Eq. (2) is determined one after the other in an incremental way, in a so-called *greedy* process.

Let us suppose the decomposition is known until $m-1$ terms, such that one can write:

$$s_m(t) = s_{m-1}(t) + \alpha_m \Psi(t - \tau_m) \tag{3}$$

where the remaining unknown correspond to α_m and τ_m. The unknowns of Eq. (3) are determined in a way such that they minimize an error

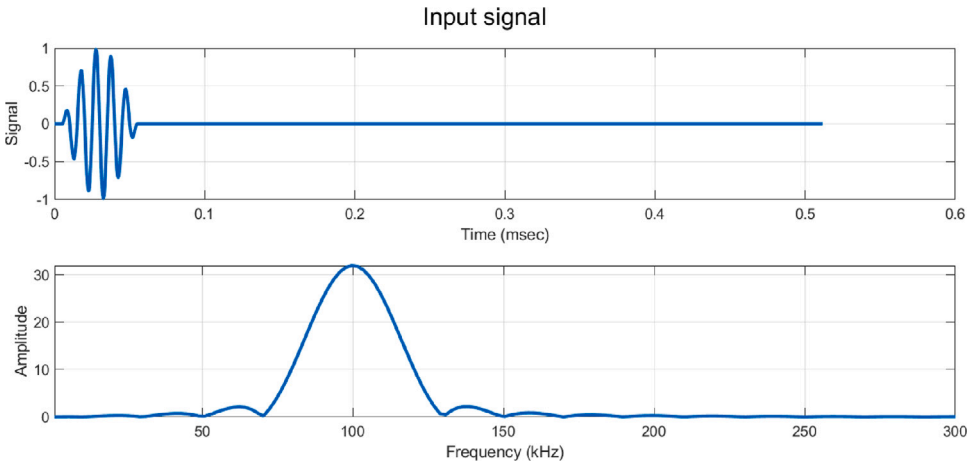

Fig. 1. Typical input signal used for LW SHM purposes. Here the central frequency f_0 is 100 kHz and the burst is composed of 5 cycles with a half-sinusoidal window.

between the approximation and the reference signal. This error can be defined in time as follows:

$$\{\alpha_m, \tau_m\} = \underset{\{\alpha_m,\tau_m\}}{\arg\min} \left\| \alpha_m \Psi(t-\tau_m) - s_{res}^{m-1}(t) \right\|_{I_t}^2 \tag{4}$$

where $s_{res}^{m-1}(t)$ corresponds to the residual signal, and is therefore given as follows:

$$s_{res}^{m-1}(t) = s(t) - s_{m-1}(t) \tag{5}$$

and the used norm is defined as follows:

$$\|\cdot\|_{I_t}^2 = \int_{I_t} (\cdot)^2 dt \tag{6}$$

with the temporal domain $I_t = [0, T]$.

The minimization problem defined by Eq. (4) can also be defined in the frequency domain using the Parseval's theorem:

$$\{\alpha_m, \tau_m\} = \underset{\{\alpha_m,\tau_m\}}{\arg\min} \left\| \alpha_m \hat{\Psi}(\omega) e^{-j\omega\tau_m} - \hat{s}_{res}^{m-1}(\omega) \right\|_{I_\omega}^2 \tag{7}$$

with $\hat{\bullet} = \mathcal{F}(\bullet)$ (Fast Fourier Transform) and its corresponding norm defined in the frequency domain:

$$\|\cdot\|_{I_\omega}^2 = \int_{I_\omega} (\cdot)^*(\cdot) d\omega \tag{8}$$

where $(\cdot)^*$ corresponds to the complex conjugate of $(\cdot)$.

The physical meanings of the quantities of interest either in the temporal of the frequency domain are here very similar. Indeed, the features being sought correspond to a scalar amplitude α and a time delay τ. As the Fourier transform is a linear operator, the scalar amplitude remains the same in both domains and thus its interpretation is similar in time or frequency. The temporal delay τ corresponds to the propagation time in the time domain and is associated with a $exp(-j2\pi f\tau)$ term in the frequency domain. In the frequency domain, it thus just corresponds to an additional linear phase that has a slope proportional to the time delay τ [34].

2.3. Optimal determination of amplitudes α_m and phases τ_m

A simple numerical algorithm is presented here, allowing to obtain the optimal amplitudes and phases for the term m of the decomposition in the sense of Eq. (7). For this, first let us notice that by minimizing the functional of Eq. (7) with respect to the amplitude α_m by employing variational calculus [35], one obtains: $\forall \delta\alpha \in \mathbb{R}$,

$$\int_{I_\omega} \delta\alpha_m \left(\hat{\Psi}(\omega) e^{-j\omega\tau_m} \right)^* \left(\alpha_m \hat{\Psi}(\omega) e^{-j\omega\tau_m} - \hat{s}_{res}^{m-1}(\omega) \right) d\omega = 0 \tag{9}$$

which directly implies:

$$\alpha_m(\tau_m) = \frac{\mathrm{Re}\left(\int_{I_\omega} \left(\hat{\Psi}(\omega) e^{-j\omega\tau_m} \right)^* \hat{s}_{res}^{m-1}(\omega) d\omega \right)}{\int_{I_\omega} \left(\hat{\Psi}(\omega) e^{-j\omega\tau_m} \right)^* \left(\hat{\Psi}(\omega) e^{-j\omega\tau_m} \right) d\omega} \tag{10}$$

where $\mathrm{Re}(\bullet)$ represent here the real part of $\bullet$. Eq. (10) gives the optimal amplitude by minimizing Eq. (7) with respect to any value of τ_m. The real part function is used in Eq. (10) since $\alpha_m(\tau_m)$ is a real number.

Now that we know for a given delay τ_m the optimal amplitude $\alpha_m(\tau_m)$ to retain, let us minimize the error norm with respect to the time phase τ_m. To do so, let us first notice that by developing Eq. (7), one obtains:

$$\begin{aligned} &\left\| \alpha_m \hat{\Psi}(\omega) e^{-j\omega\tau_m} - \hat{s}_{res}^{m-1}(\omega) \right\|_{I_\omega}^2 = \\ &\left\| \alpha_m \hat{\Psi}(\omega) e^{-j\omega\tau_m} \right\|_{I_\omega}^2 - g(\alpha_m, \tau_m) + \left\| \hat{s}_{res}^{m-1}(\omega) \right\|_{I_\omega}^2 \end{aligned} \tag{11}$$

with:

$$g(\alpha_m, \tau_m) = 2\alpha_m \mathrm{Re}\left(\int_{I_\omega} \left(\hat{\Psi}(\omega) e^{-j\omega\tau_m} \right)^* \hat{s}_{res}^{m-1}(\omega) d\omega \right) \tag{12}$$

If one injects the expression of the amplitude $\alpha_m(\tau_m)$ from Eq. (10) that minimizes the error norm, into Eq. (11) one obtains after simplification:

$$\left\| \alpha_m \hat{\Psi}(\omega) e^{-j\omega\tau_m} - \hat{s}_{res}^{m-1}(\omega) \right\|_{I_\omega}^2 = \left\| \hat{s}_{res}^{m-1}(\omega) \right\|_{I_\omega}^2 - G(\tau_m) \tag{13}$$

where:

$$G(\tau_m) = \frac{\left[\mathrm{Re}\left(\int_{I_\omega} \left(\hat{\Psi}(\omega) e^{-j\omega\tau_m} \right)^* \hat{s}_{res}^{m-1}(\omega) d\omega \right) \right]^2}{\int_{I_\omega} \left(\hat{\Psi}(\omega) e^{-j\omega\tau_m} \right)^* \left(\hat{\Psi}(\omega) e^{-j\omega\tau_m} \right) d\omega} \tag{14}$$

From Eq. (13), one can clearly recognize that the value of τ_m that minimizes the error simply corresponds to the one that maximizes $G(\tau_m)$. The optimal value of τ_m can be easily computed as $G(\tau_m)$ is a one-dimensional function. From the optimal value of the time phase τ_m, the amplitude α_m is finally determined via Eq. (10).

2.4. Convergence and the stop criterion

The procedure of computing each of the terms of Eq. (2) is performed until a given approximation error is reached. This error is defined as follows:

$$\xi_m = 100 \times \frac{\left\| \sum_{i=1}^{m} \alpha_i \Psi(t-\tau_i) - s(t) \right\|_{I_t}}{\|s(t)\|_{I_t}} \tag{15}$$

2.5. Overview of the SAMPM algorithm

A schematical overview of the SAMPM workflow is provided in Fig. 2.

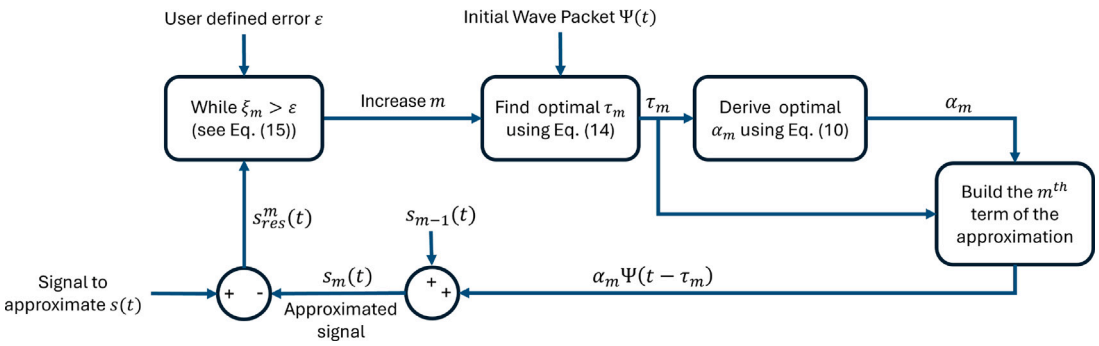

Fig. 2. Schematical overview of the SAMPM algorithm workflow.

3. Single atom convolutional matching pursuit

In order to better approximate the dispersion phenomena observed on signals under the SAMPM rationale proposed in the previous Section, we propose here to include a convolution operation, allowing taking into account the dispersion effect on the selected initial atom during its propagation over the structure to monitor.

3.1. Problem statement

Dispersive phenomena correspond in practice to a spread of the IWP during its propagation. This is due to the fact that all the frequencies do not propagate at the same phase and group velocities in presence of dispersion. For the antisymmetric mode A_0 for example, low frequencies are usually traveling slower than high frequency ones. In terms of signal processing, if all the frequencies are traveling with a constant speed, it can be interpreted as a linear filtering operation with a linear phase in the frequency domain. As in the dispersive case all the frequencies are not propagating with a similar velocity, this can then be interpreted still as a linear filtering operation with nonlinear phase in the frequency domain. We thus have chosen to model the effect of dispersion as a general linear convolution that can handle the expected effects in terms of signal processing and the only underlying assumption we made is that dispersion can be modeled as a linear filtering operation which is rather classical [36,37].

Here, we propose the following decomposition:

$$s(t) \approx s_m(t) = \sum_{i=1}^{m} \left[\alpha_i(t) * \Psi(t-\tau_i)\right](t) \tag{16}$$

where $*$ corresponds to the convolution operator, defined as follows:

$$(f * g)(t) = \int_{-\infty}^{\infty} f(s)g(t-s)ds \tag{17}$$

Thus, from the above definition, if we denote $\Psi_{\tau_i}(t) = \Psi(t-\tau_i)$ (the input signal $\Psi(t)$ delayed by the quantity τ_i), the operation in Eq. (16) simply consists of:

$$\left[\alpha_i(t) * \Psi(t-\tau_i)\right](t) = \int_{-\infty}^{\infty} \alpha_i(s)\Psi_{\tau_i}(t-s)ds \tag{18}$$

On this proposed decomposition, one considers no longer a scalar amplitude α_m multiplying the delayed atom but rather a temporal signal $\alpha_m(t)$ being convolved with the delayed atom. Furthermore, this temporal signal $\alpha_m(t)$ can be interpreted as an impulse response relating the mth wave packet to the delayed initial atom due to the fact that a convolution operation is used between $\alpha_m(t)$ and the atom $\Psi(t-\tau)$. Consequently, the family of $\alpha_m(t)$ will be called the wave packets impulse responses. In this work, the proposed decomposition is called Single Atom Convolutional Matching Pursuit method (SACMPM).

3.2. Wave packets impulse responses approximation

Here the wave packets impulse responses are approximated by using Chebyshev polynomials of the second kind. Therefore one has:

$$\alpha_m(t) = \sum_{i=1}^{N} N_i(t)\beta_i = \underline{\boldsymbol{N}}(t)^T\underline{\boldsymbol{\beta}} \tag{19}$$

where, β_i and $N_i(t)$ correspond to the weight (of each shape function) and the shape function, respectively. This choice of approximation of the time function is made due to the simplicity of the implementation and improved conditioning of the operators needed to be inverted.

Remark. Here, because the used atom has a local support in time (interval size where the function is defined), the function $\alpha(t)$ has consequently this same interval of definition.

3.3. Greedy construction of the decomposition

Following the same strategy as the one exposed for SAMPM, here, the wave packet impulse responses $\alpha_i(t)$ and the time-delays of the atom τ_i are computed in a greedy way. In this sense, let us suppose the decomposition known until $m-1$ terms, such that we can write:

$$s_m(t) = s_{m-1}(t) + \left[\alpha_m(t) * \Psi(t-\tau_m)\right](t) \tag{20}$$

therefore, the main unknowns are computed by minimizing the following norm:

$$\{\alpha_m, \tau_m\} = \underset{\{\alpha_m,\tau_m\}}{\arg\min} \left\| \left[\alpha_m(t) * \Psi(t-\tau_m)\right](t) - s_{res}^{m-1}(t) \right\|_{I_t}^2 \tag{21}$$

with $s_{res}^{m-1}(t) = s(t) - s_{m-1}(t)$.

3.4. Determination of temporal time delays τ_m

The temporal delays are determined exactly in the same way as exposed in Section 2.3 by assuming a constant amplitude α_m. The main reason motivating this choice is based on the fact that obtaining an optimal solution of wave packet impulse responses and time delay is really complicated based on iterative resolution methods applied to Eq. (21), due to ill-conditioning of the operators needed to be inverted, in addition, the iterative procedure is completely eliminated since τ is computed directly.

3.5. Determination of the wave packet impulse responses $\alpha_m(t)$ given τ_m

Given τ_m, the temporal function $\alpha_m(t)$ is computed such as it minimizes Eq. (21). By minimizing with respect to this function [35], it results:

$$\forall \delta\alpha_m(t),$$
$$\int_{I_t} \left[\delta\alpha_m(t) * \Psi(t-\tau_m)\right](t) \left(\left[\alpha_m(t) * \Psi(t-\tau_m)\right](t) - s_{res}^{m-1}(t)\right) dt = 0 \tag{22}$$

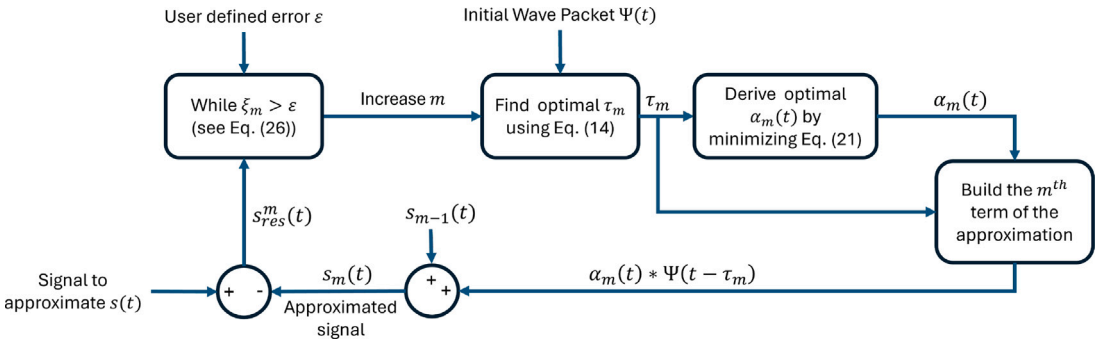

Fig. 3. Schematical overview of the SACMPM algorithm workflow.

By introducing Eq. (19) into Eq. (22), one obtains the following matrix equation:

$$\underline{\underline{\boldsymbol{M}}}\,\underline{\boldsymbol{\beta}} = \underline{\boldsymbol{F}} \tag{23}$$

with the matrix $\underline{\underline{\boldsymbol{M}}}$ and vector $\underline{\boldsymbol{F}}$ given by:

$$\underline{\underline{\boldsymbol{M}}} = \int_{I_t} \underline{\boldsymbol{B}}(t)\,\underline{\boldsymbol{B}}(t)^T dt \quad \text{and} \quad \underline{\boldsymbol{F}} = \int_{I_t} \underline{\boldsymbol{B}}(t)\, s_{res}^{m-1}(t) dt \tag{24}$$

where the shape functions are given by:

$$\underline{\boldsymbol{B}}(t) = \left[\underline{\boldsymbol{N}}(t) * \Psi(t-\tau_m)\right](t) \tag{25}$$

3.6. Convergence and the stop criterion

New terms are added to the decomposition until a given approximation error is reached. This error is defined as follows:

$$\xi_m = 100 \times \frac{\left\| \sum_{i=1}^{m} \left[\alpha_i(t) * \Psi(t-\tau_i)\right](t) - s(t) \right\|_{I_t}}{\|s(t)\|_{I_t}} \tag{26}$$

3.7. Overview of the SACMPM algorithm

A schematical overview of the SACMPM workflow is provided in Fig. 3.

4. Efficiency of SAMPM and SACMPM applied to numerical and experimental LW-based SHM signals

In this Section, the previously presented decomposition algorithms (namely SAMPM and SACMPM see Sections 2 and 3) will be applied to approximate signals which are representative of LW based SHM applications. Firstly, numerical signals corresponding to LW propagation in an infinite isotropic plate will be considered in Section 4.1. Then SAMPM and SACMPM will be applied to experimental signals collected on the fan cowl part of an A380 nacelle in Section 4.2.

4.1. Numerical example

4.1.1. Simulated signals to be approximated

As a first step to demonstrate the decomposition abilities of the SAMPM and SACMPM algorithms a very simple numerical case is considered. This case consists of the propagation of A_0 and S_0 modes in an infinite thin plate, and details regarding the simulation are provided in Appendix A.

The numerical signal consist of 1024 samples, with a sampling frequency of 2 MHz, and correspond to an input having a central frequency f_0 = 100 kHz and with 5 cycles bursts. Signals have been computed for distances d ranging from 15 cm to 55 cm by step of 5 cm. Such distances are quite common in practice for the LW based SHM of aeronautic composite structures, as will be shown later. The resulting signals corresponding to these computations are shown in Fig. 4. As can be seen from this figure, the signals are made up of 2 wave packets: the first one, the fastest, corresponds to S_0, and the second one, the slowest, to A_0. As expected from the dispersion curves analysis shown in Appendix A, the S_0 wave packet does not suffer from dispersion, whereas the A_0 one is distorted during propagation because of dispersion.

4.1.2. Comparison of SAMPM and SACMPM methods performances

The SAMPM and SACMPM algorithms described in Sections 2 and 3 have then been applied to the simulated signals described previously with an initial atom corresponding to the input signal existing the structure. For the SACMPM method, the discretization parameter N has been set to 40. A maximum of 50 terms of the decomposition has been allowed, and convergence was supposed to be reached when the error was lower than 10%. One should keep in mind that as two wave packets are physically propagating here, the minimum number of terms that could be found by either SAMPM or SACMPM is 2.

A comparison of the performances of the SAMPM and SACMPM algorithms for the simulated signals corresponding to different propagation distances is shown in Fig. 5. From this figure, it can be observed that using the input signal as the initial atom both algorithms converge to an error lower than 10% with 3 and 4 terms for propagation distance corresponding to 15 cm, 20 cm, and 25 cm. According to Fig. 4, for those propagation distances, the two wave packets to be identified are either mixed (15 cm) or very close to each other (20 cm and 25 cm). Results provided by SAMPM and SACMPM are thus acceptable. For larger distances ($d \geq 25$ cm), SACMPM converges with fewer terms than SAMPM. In those cases, the wave packets to be identified are well separated according to Fig. 4. The fact that SAMPM needs more terms to converge is related to the fact that this algorithm is not able to learn, dispersion whereas SACMPM can.

The approximated signal as well as the first 6 terms obtained using the SAMPM for the signal corresponding to a propagation distance of 45 cm are shown in Fig. 6. From this figure, it can be seen that for an error lower than 10%, the approximation provided by SAMPM is extremely satisfying. It can also be seen that the first term of the decomposition corresponds exactly to the propagated S_0 mode. This was to be expected as the SAMPM algorithm just propagates the input signal without dispersion and as the S_0 mode does not endure dispersion. The second term being identified by the SAMPM algorithm corresponds, however, roughly to the second propagating term. This was also expected as this term is a propagated version of the input signal but with some dispersion effects. Consequently, it resembles the input signals but with some differences that can clearly be seen here. The terms 3, 4, and 5 then seek to correct the small mismatches between the translated input signal and the actually observed second wave packet. Finally, the term number 6 corrects some very small amplitude mismatches obtained in the first wave packet.

The approximated signal, as well as the first 3 terms obtained using the SACMPM for the signal corresponding to a propagation distance of 45 cm are then shown in Fig. 7. Again, the approximation provided by SACMPM is extremely satisfying. Furthermore, the first term almost

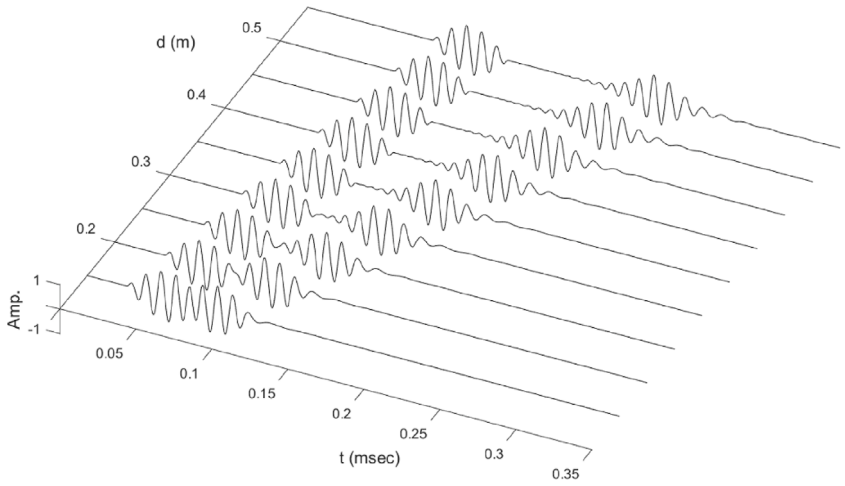

Fig. 4. Simulated signals for various propagating distances.

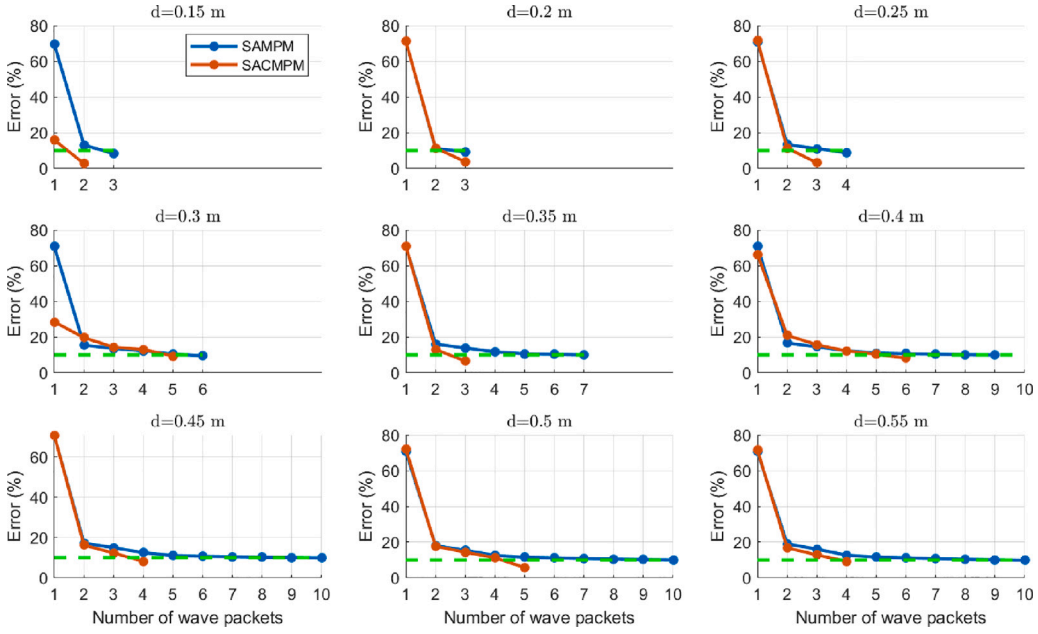

Fig. 5. Comparison of the performances of the SAMPM and SACMPM algorithms for the simulated signals corresponding to different propagation distances.

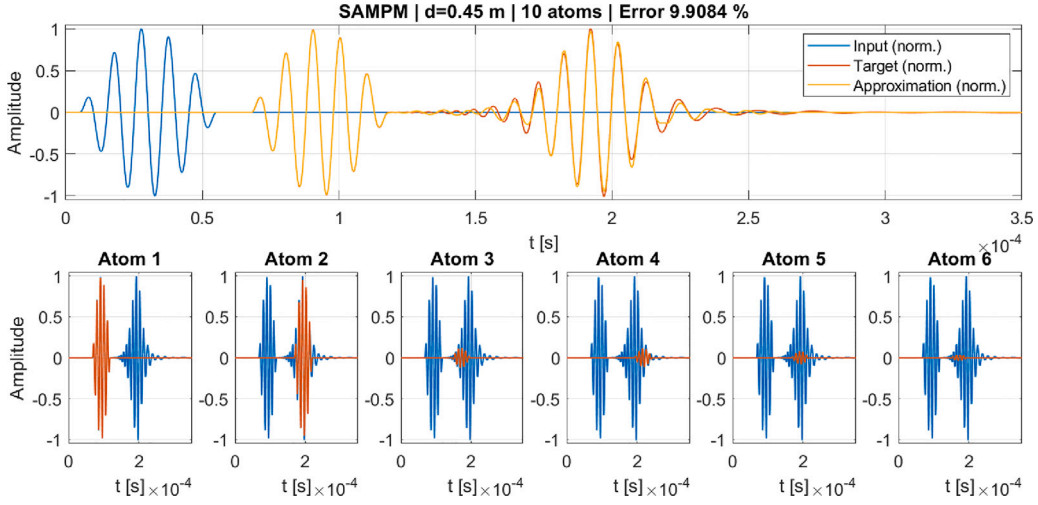

Fig. 6. *[Top]* Input signal, target signal, and approximated signal using the SAMPM algorithm with 10 terms. *[Bottom]* First 6 terms (in red) obtained using the SAMPM for the signal corresponding to a propagation distance of 45 cm. Convergence with a 10% error was not reached with three terms, but ten terms are required.

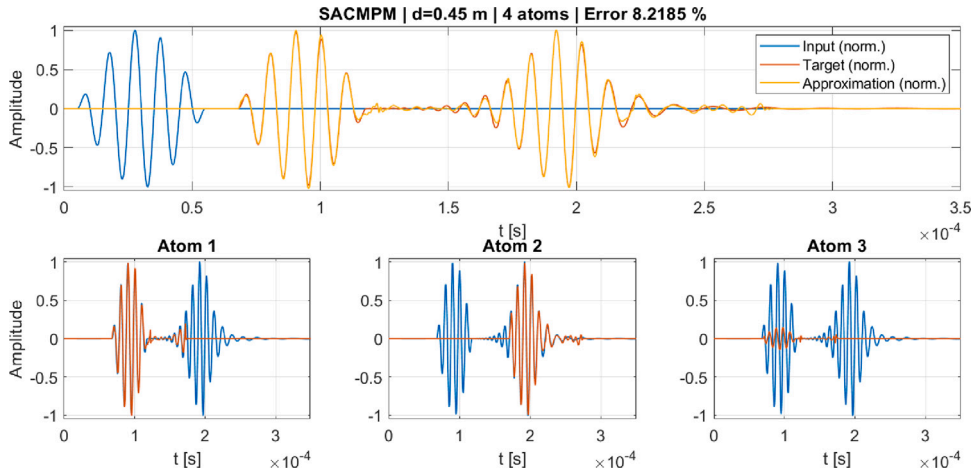

Fig. 7. *[Top]* Input signal, target signal, and approximated signal using the SACMPM algorithm with 4 terms. *[Bottom]* First 3 terms (in red) obtains using the SACMPM for the signal corresponding to a propagation distance of 45 cm. Convergence with a 10% error was reached with four terms.

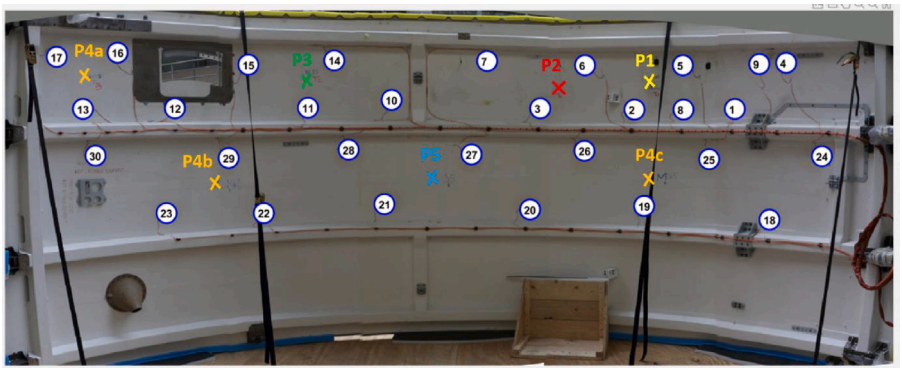

Fig. 8. Overview of the geometrical configuration of the Fan Cowl Structure (FC) experimental datasets.

perfectly corresponds to the first wave packet to approximate, as expected. The second term also almost perfectly corresponds to the second wave packets. Now that convolution has been included in the SACMPM algorithm, it is possible to better represent the dispersive behavior of the signal, as illustrated here.

4.1.3. Overview

In summary, it is demonstrated here in this simple simulated example, which is representative of the targeted LW based SHM application, but includes only two wave packets that both the SAMPM and the SACMPM algorithms are able to efficiently approximate the target signals. Furthermore, as the SACMPM algorithm allows for compensation of the dispersion effects, it is more efficient than the SAMPM algorithm in doing so.

4.2. Experimental example

4.2.1. Considered experimental data: fan cowl of the a380 fan cowl structure

The aeronautics structure under study experimentally consists here in the fan cowl part of a nacelle of an Airbus A380 as shown in Fig. 8. The experimental details related to the structure under study are given in Appendix B. The considered experimental signals are shown in Fig. 9. From this figure, it can be observed that the experimental signals are not as simple as the simulated ones previously presented. Indeed, in addition to the two initially propagating modes A_0 and S_0, reflections coming from structural boundaries and inhomogeneities such as the stiffeners (see Fig. 8) generate additional wave packets that are also caught by the receiving piezoelectric elements. One can also notice that due to damping present in composite materials, the amplitude of the first peak decreased with increasing propagating distance. This structure has already been used by the authors for other studies, and more details can be found in related works [38–40].

4.2.2. Comparison of SAMPM and SACMPM methods performances

The SAMPM and SACMPM algorithms described in Sections 2 and 3 have then been applied to the experimental signals described previously. As previously, for the SACMPM method, the discretization parameter N has been set to 40. A maximum of 100 terms has been allowed to approximate the experimental signals.

A comparison of the performances of the SAMPM and SACMPM algorithms for the experimental signals corresponding to different propagation distances are shown in Fig. 10. From this figure, it can be observed that given 100 terms, SAMPM converges to an error of roughly 50%, whereas SACMPM converges to an error of $\simeq$ 20% for all distances. In that case, convergence is faster for SACMPM than for SAMPM for all the tested distances. This can be again interpreted by the fact that SACMPM is able to take into account dispersion during its estimation process, whereas SAMPM cannot. Convergence curves associated with SAMPM are, however, smoother than the ones of SACMPM. This can be attributed to the fact that the way SAMPM is being solved always ensures that the optimal amplitude and the best delay for a given atom are found. For SACMPM, some bumps can be observed in the convergence curves; this is mainly due to the fact that the time function $\alpha(t)$ (which is convolved with the atom) is built on a basis, which may penalize the approximation a little if the signal to be processed has a rich and complex frequency content. However, its global approximation for a fixed number of terms in the decomposition is always guaranteed

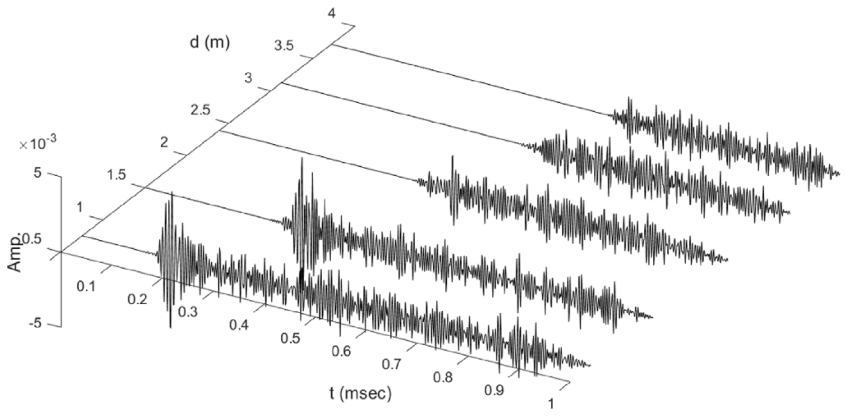

Fig. 9. Experimental signals for various propagating distances.

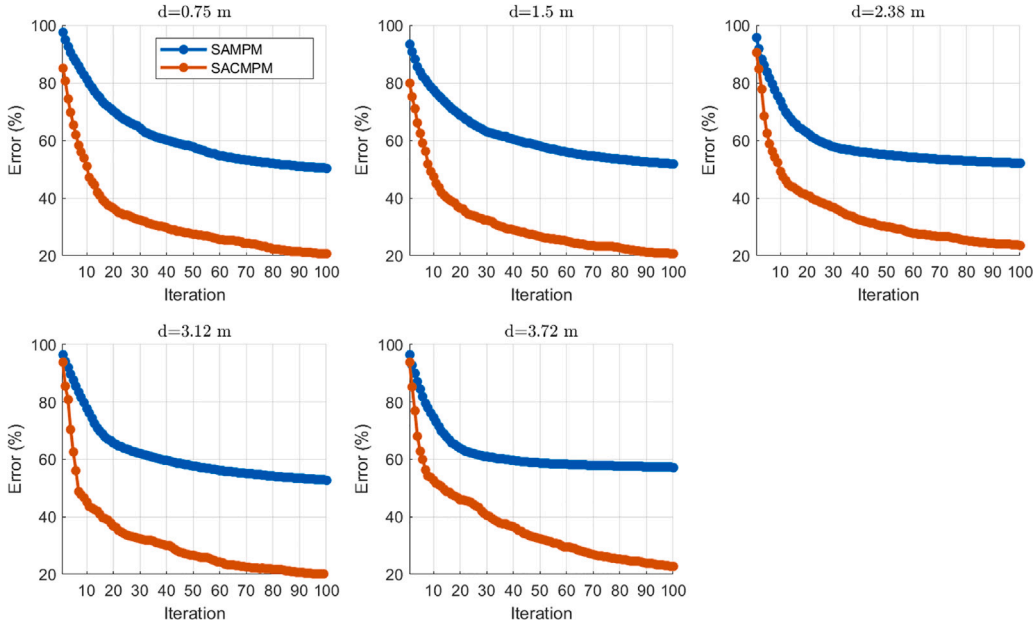

Fig. 10. Comparison of the performances of the SAMPM and SACMPM algorithms for the approximation of experimental signals corresponding to different propagation distances.

to be better than SAMPM by construction. The approximated signal, as well as the first 6 terms obtained using the SAMPM for the signal corresponding to a propagation distance of 1.5 m are then shown in Fig. 12. The approximation provided by SAMPM is satisfactory given the complexity of signals at hand, even if the error at the end is of $\simeq$ 50%. Interpretation of the terms being found is here, however, trickier given the complexity of the structure at hand. The approximated signal, as well as the first 6 terms obtained using the SACMPM for the signal corresponding to a propagation distance of 1.5 m are then shown in Fig. 12. Again, the approximation provided by SACMPM is very satisfying given the complexity of signals at hand, even if the error at the end is of $\simeq$ 20%. Interpretation of the terms being found is, here again, quite tricky, given the complexity of the structure at hand. The first and fifth terms seem to be related to the wave packet corresponding to the S_0 mode. Interestingly, the third and fourth wave packets seem to be associated with the A_0 mode wave packet. This suggests that on these experimental signals, SACMPM allows us to better catch the physics behind the analyzed signals than SAMPM.

4.2.3. Overview

In summary, the analysis of the experimental signals that have been carried out suggests that SAMPM and SACMPM can be used for the analysis of signals coming from complex structures. The error rate obtained here with 100 terms is not extremely low ($\simeq$ 50% for SAMPM and $\simeq$ 20% for SACMPM), but the visual results presented in Figs. 11 and 12 suggest that the approximation is very good, catching the main features of the signal. As expected by the fact that SACMPM incorporates the ability to model dispersion, its convergence rate is better than that of SAMPM. In terms of physical interpretability, the results provided by the SACMPM better corroborate with the expectations that one can have regarding the first S_0 and A_0 wave packet propagation in such a structure.

5. Damage localization using SAMPM and SACMPM features

In order to demonstrate the practical usefulness of the proposed signal approximation techniques for LW-based SHM purposes, this section aims at localizing damage in a structure using features obtained after SAMPM and SACMPM decomposition of LW signals that are then fed to a neural network.

5.1. Numerical database of LW-based SHM signals

The structure under study is now a $300 \times 300 \times 2.4$ mm^3 plate made up of a composite material representative of the aeronautic industry.

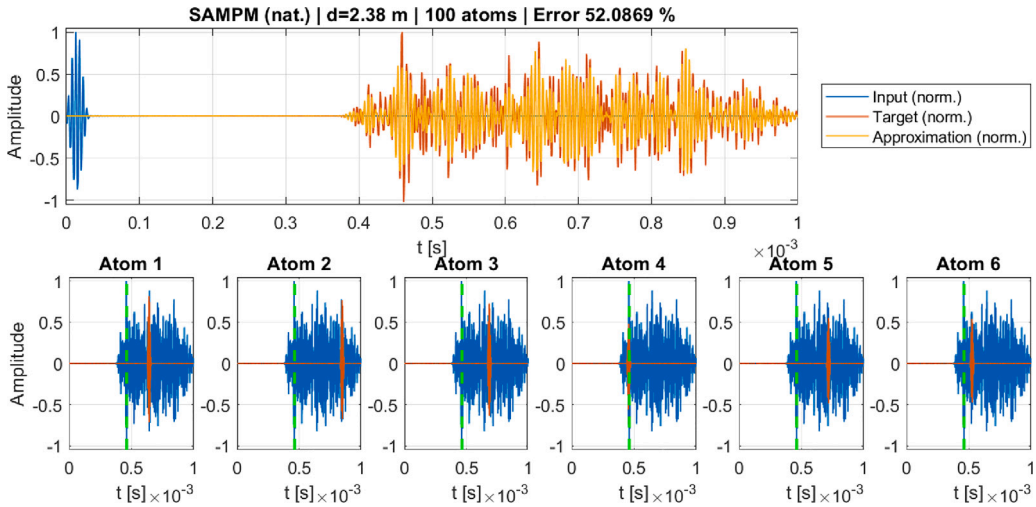

Fig. 11. *[Top]* Input signal, target signal, and approximated signal using the SAMPM algorithm with 100 terms. *[Bottom]* First 6 terms (in red) obtains using the SAMPM for the signal corresponding to a propagation distance of 1.5 m. The green and magenta vertical lines denote the expected arrival times of the waves packets corresponding to the S_0 and A_0 modes.

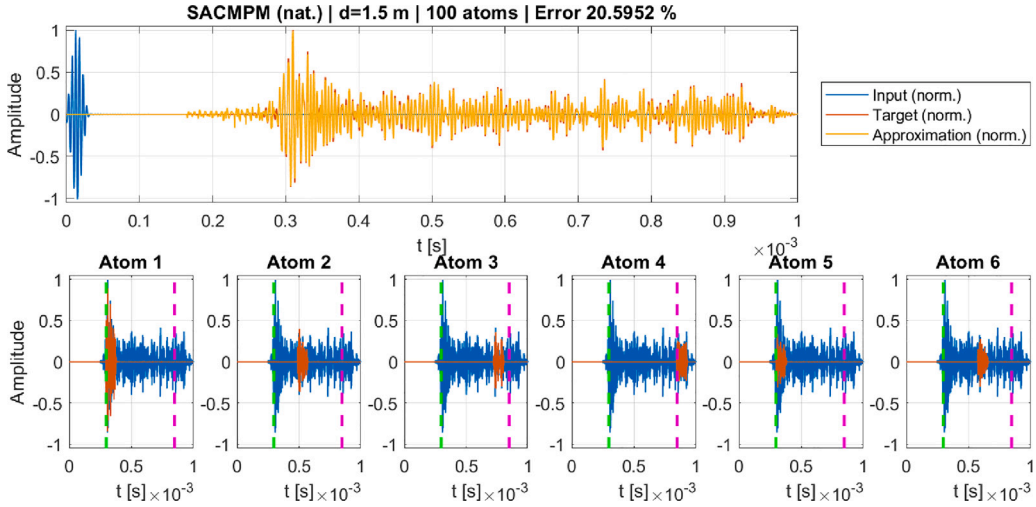

Fig. 12. *[Top]* Input signal, target signal, and approximated signal using the SAMPM algorithm with 100 terms. *[Bottom]* First 6 terms (in red) obtained using the SACMPM for the signal corresponding to a propagation distance of 1.5 m. The green and magenta vertical lines denote the expected arrival times of the waves packets corresponding to the S_0 and A_0 modes.

Fig. 13 illustrates the disposition of PZTs as well as one damage on the simulated structure, and computational details are provided in Appendix C.

5.2. Problem statement

A machine learning approach consisting of a feedforward neural network (NN) is considered for damage localization purposes using features extracted from LW signals using either SAMPM or SACMPM described previously.

As input for the NN, one thus considers the constant amplitude for SAMPM or the wave packet impulse responses for SACMPM and the time delays $\{\alpha_k(t), \tau_k\}_{k=1}^{m}$ with m the number of terms in the approximation when SAMPM or SACMPM are applied to the signal created as the difference between an *undamaged* and *damaged* response of the LW measured by PZTs distributed in the structure. No preselection of features have been previously achieved. The neural network has been provided with all the available information after the decompositions have been carried out.

To compare both methods, here we considered $m = 6$ terms for both methods for all treated signals. As output of the NN, one considers the damage location expressed here as $\underline{x}$. In this sense, for the damage localization, one considers the following neural network mapping NN(·):

$$\mathrm{NN}(\{\alpha_k(t), \tau_k\}_{k=1}^{m}) \rightarrow \underline{x}_{\mathrm{pred}} \tag{27}$$

where, $\underline{x}_{\mathrm{pred}}$ denotes the predicted location of damage.

The architecture considered for the neural network consists of a feed forward network, with 3 hidden layers, where each layer has 150 neurons. The activation functions considered are hyperbolic tangent (*tanh*), and the output activation function is linear. As training data, 37 data points are considered, while 5 are used as test data.

The operation process simply consists of training a neural network using the features extracted as input from signals measured by PZTs when damage is present in the structure. The idea is that the neural network will be able to learn the relationship between features and damage location. Once the network is trained, it is then used as a damage detection tool for scenari where there is another damage configuration that has not been considered in the training. Thus, for this new configuration, the structure is firstly excited by means of ultrasonic Lamb waves and the signals measured by sensors are

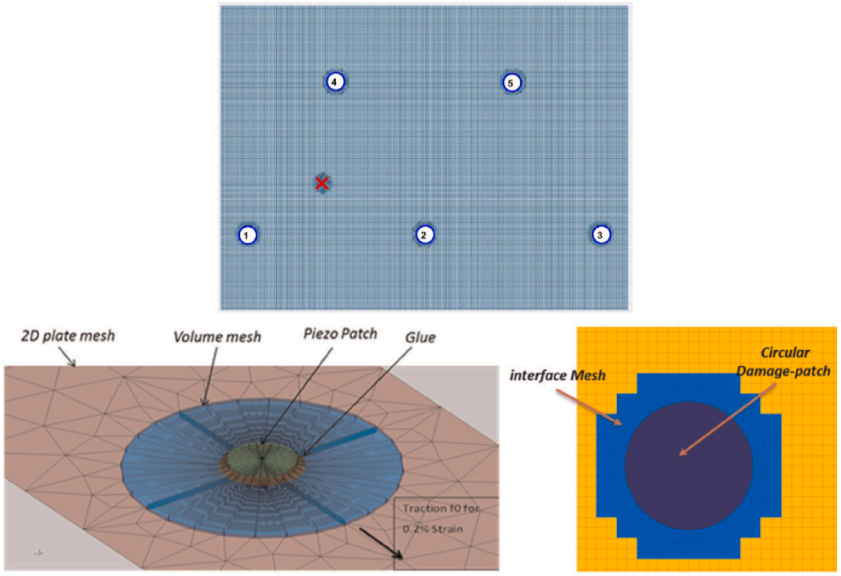

Fig. 13. *[Left]* Overview of the geometrical configuration for the simulated database. Mesh details around the PZT element *[Center]* and the damage *[Right]*.

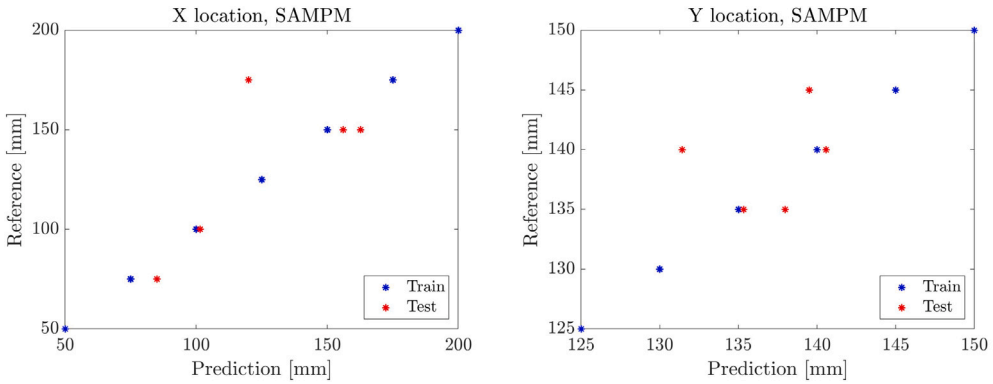

(a) (b)

Fig. 14. Damage location prediction for train and test data when using the SAMPM.

Table 1
Error for the prediction of damage location by using the features of SAMPM and SACMPM.

Method	Test error x coordinate [%]	Test error y coordinate [%]
SAMPM	3.44	19.63
SACMPM	3.18	13.76

recorded. Secondly, the SAMPM or SACMPM decomposition is applied to the recorded signals and its features are extracted. Finally the neural network is used, where the features are the input of the network and the output is the final prediction of the damage location for this new configuration.

5.3. Damage localization results

The prediction of damage location given by the NN for the training as well as the test data-set for the SAMPM are presented in Fig. 14. On the other hand, the results corresponding to SACMPM are presented in Fig. 15. The prediction results of damage location in terms of relative errors (i.e. the relative difference between the estimated damage location and the actual damage location) provided by the NN by using the features of the SAMPM and SACMPM are summarized in Table 1.

From the results presented in Table 1, one can conclude that the SAMPM allows obtaining good features in order to produce damage identification, however, since the identification error associated with the SACMPM is lower, this means this decomposition allows obtaining richer features, that are more efficiently used by the NN for damage localization purposes.

6. Discussion

6.1. Usefulness of SAMPM and SACMPM in other application fields

Although the signal approximation methods proposed in this paper find an original application in the context of LW-based SHM, these techniques are rather general and can be easily applied to a large class of signal processing problem. Indeed, the proposed algorithmic approaches only assume that the signals that are collected by whatever sensing technology originate from a single atom after propagation in a dispersive and attenuative media. Thus, many different single atom types can be easily and naturally considered by the method: pulse, chirp, burst, impulse, etc. The method is thus extremely general from a first point of view as it can cope with many types of different input signals. As a perspective for future work, it is considered to provide the online calculation of atoms together with the SAMPM and SACMPM, where these atoms would allow to better approximate the reference signals and obtain in parallel an extraction of better features to improve the damage identification.

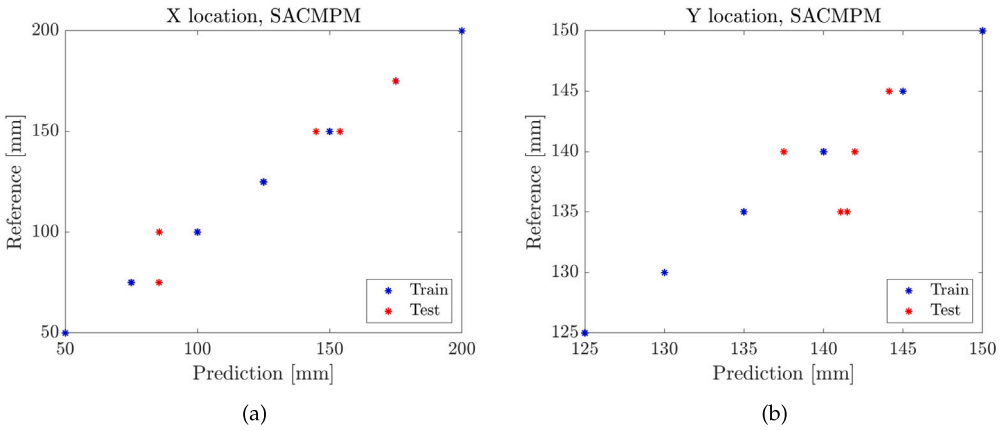

Fig. 15. Damage location prediction for train and test data when using the SACMPM.

Furthermore, the applications of SAMPM or SACMPM can be the same as the ones targeted by classical matching pursuit method under the constraints that a single atom is generating the resulting signals after propagation in a dispersive and attenuative media. This encompasses for example non-destructive testing using ultrasound [41], medical ultrasounds [42], undersea ultrasounds [43], room acoustics [44,45], electromagnetic radars [36,37], etc. If one takes room acoustics as an example, acoustical wave propagation in air is unimodal and non-dispersive. It thus corresponds to a simplified case in comparison with the one addressed here from that point of view. However, the aim of room acoustics is to model the acoustical interactions between a source located in space and its surrounding environment, like walls, ceiling, floor, etc. Thus, instead of being a 2D problem, it becomes a 3D problem and thus potentially more reflections will need to be considered. Finally, one simple way to perform room acoustic measurements is to pop a balloon at a given position and to measure the resulting signals at various other positions. Here, the initial wave packet corresponds to the initial pop that will then propagate in air and interact with all the architectural details of the room to be acoustically modeled. The proposed SAMPM algorithm can thus be directly used in such a context. It is thus believed that many application fields can benefit from the SAMPM and SACMPM algorithms.

6.2. Towards physically informed and understandable signal decomposition

As mentioned in Section 1, many methods already exists in the bibliography that seems applicable for the decomposition of Lamb waves or more generally signals having a physical origin. Those methods rely principally on mathematical strong basis rather than on a physical interpretative basis. This can be very usefully in some context where dimension reduction or data compression applications are targeted. However, this severely limits their practical usefulness for application where the physical behavior associated with the signals history has to be understood, as in LW-based SHM. Indeed, the results provided by mathematical approaches of signal decomposition are almost impossible to physically interpret and to understand thus drastically limiting their explainability. In the proposed approach, the main objective consisted in enriching the numerical approximation with a physical understanding of the decomposition coupled with some physical assumptions, thus allowing to interpret and understand the obtained decomposition. At the end, each term of the obtained decomposition can potentially be linked with a given propagation path and thus with a given time history within the monitored thin structures.

7. Conclusions and perspectives

Classical matching pursuit algorithm decomposes a given signal as a sum of delayed and scaled atoms taken out of an a priori learnt dictionary. This approach is not suitable for many physical signals and in particular for signals propagating in a dispersive and attenuating medium, as it is the case for Lamb waves being used for the structural health monitoring of composite thin structures.

The contributions of this article can be summarized as follows:

- The first contribution of the present paper is to introduce a mathematical framework called Single Atom Matching Pursuit Method (SAMPM) allowing to approximate Lamb waves based structural health monitoring signals without the need for a predefined dictionary.
- As a second contribution, this idea is extended to take into account dispersive phenomena and the proposed extension is called Single Atom Convolutional Matching Pursuit Method (SACMPM). The main idea of SACMPM consists of decomposing a measured signal as a delayed atom convolved with temporal functions, being richer features allowing to model dispersion effects on the input signal.
- In order to demonstrate the interest of those algorithms, the SAMPM and SACMPM methods were successfully applied to approximate numerical signals as well as signals measured experimentally.
- Finally, it has been demonstrated that the features extracted from both methods can also be used as input to feed a neural network to predict damage location, where good predictions were obtained which makes SAMPM and SACMPM appealing from a practical point of view.

CRediT authorship contribution statement

Sebastian Rodriguez: Writing – review & editing, Writing – original draft, Visualization, Validation, Software, Methodology, Investigation, Formal analysis, Conceptualization. **Marc Rébillat:** Writing – review & editing, Visualization, Validation, Software, Methodology. **Shweta Paunikar:** Writing – review & editing. **Pierre Margerit:** Writing – review & editing, Methodology. **Eric Monteiro:** Writing – review & editing. **Francisco Chinesta:** Writing – review & editing, Supervision. **Nazih Mechbal:** Writing – review & editing, Supervision.

Declaration of competing interest

The authors declare that they have no known competing financial interests or personal relationships that could have appeared to influence the work reported in this paper.

Acknowledgment

The European MORPHO project is gratefully acknowledged for funding this research activity.

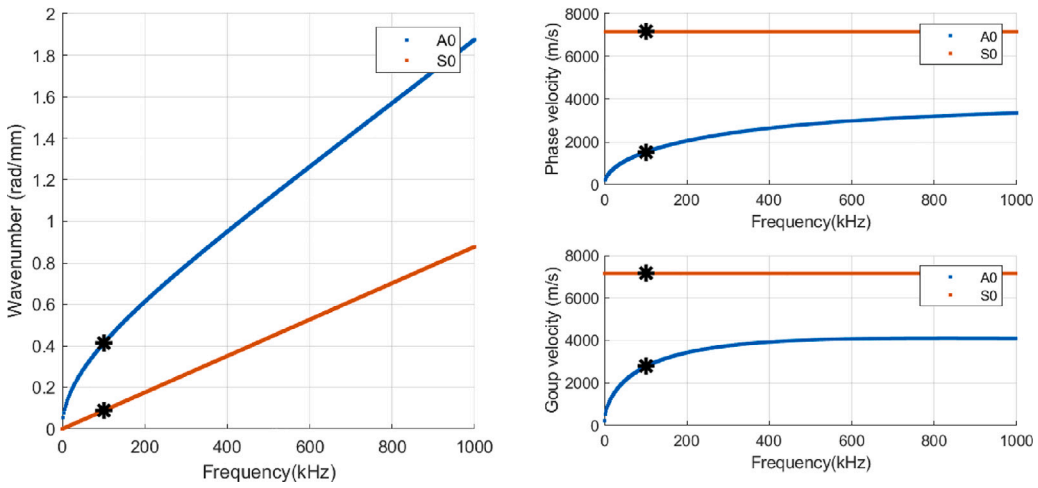

Fig. A.16. Dispersion curves for the simulated structure under study. [Left] Wavenumber k versus frequency. [Top right] Phase velocity versus frequency. [Bottom right] Group velocity versus frequency. The black symbols denotes A_0 and S_0 waves properties at the selected input frequency of $f_0 = 100$ kHz.

Appendix A. Infinite plate taken as a numerical illustrative example

The example infinite plate used for illustration has a thickness $h = 2$ mm and is made up of an isotropic material with $E = 70$ GPa, $\nu = 0.3$, and $\rho = 1500$ kg/m^3. Such a plate merely corresponds to a composite plate commonly used in aeronautic structures.

In the low frequency range of such structure, only two wave modes exist, namely the A_0 and S_0 modes, and given an input frequency f, the corresponding wavenumbers $k_{S_0}(f)$ and $k_{A_0}(f)$ can be computed as [1,9–11]:

$$k_{S_0}(f) = 2\pi f \sqrt{\frac{\rho}{Q}} \tag{A.1}$$

$$k_{A_0}(f) = \frac{2\pi f}{\sqrt{2}} \sqrt{\left(\frac{\rho}{Q} + \frac{\rho}{G\xi}\right) + \sqrt{\left(\frac{\rho}{Q} - \frac{\rho}{G\xi}\right)^2 + \frac{1}{\pi f^2}\left(\rho + \frac{\rho}{IQ}\right)}} \tag{A.2}$$

with: $G = \frac{E}{2(1+\nu)}$, $Q = \frac{E}{(1-\nu^2)}$, $\xi = \pi^2/12$, and $I = h^3/12$.

The resulting dispersion curves for the simulated structure under study are shown in Fig. A.16. On these figures, the two dispersion branches corresponding to the A_0 and S_0 modes can be seen, as well as the phase and group velocities. The phase velocity of the S_0 mode does not change with frequency, meaning that the S_0 mode does not endure dispersion, whereas the one of the A_0 mode is enduring dispersion. Furthermore, at the selected input frequency of $f_0 = 100$ kHz, it can clearly be seen that the structure is excited in a frequency region where dispersion is important for the A_0 mode.

Given an input signal $x(t)$ as the one shown in Fig. 1 (or equivalently its Fourier transform $\hat{x}(f)$), the propagated signal for a propagation distance d can be computed as:

$$s_d(t) = \sum_{n=A_0,S_0} \mathcal{F}^{-1}\left[\hat{x}(f) exp\left[-ik_n(f)d\right]\right] \tag{A.3}$$

where $\mathcal{F}^{-1}$ denotes the inverse Fourier transform. Please notice that in Eq. (A.3), it is assumed that the S_0 and A_0 modes are excited with an equal amplitude, which is not necessarily the case in practice due to the size of the PZT elements mainly. Signals have been computed using Eq. (A.3) for distances d ranging from 15 cm to 55 cm by step of 5 cm.

Appendix B. Experimental study on a A380 fan cowl structure

The fan cowl part of an Airbus A380 nacelle under study here is 1.5 m in height for a semi circumference of 4 m and is made of composite monolithic carbon epoxy material. It has been equipped with 30 PZTs manufactured by NOLIAC (diameter of 25 mm) and possesses many stiffeners delimiting various areas as shown in Fig. 8.

The excitation signal sent to the PZT element is a 5 cycled burst with an excitation frequency of $f_0 = 200$ kHz and with an amplitude of 10 V. The excitation frequency is selected to promote the mode S_0 over the mode A_0 as it propagates faster. The Lamb wave propagation speed within the material is estimated at around 5300 m/s for the S_0 mode and 1800 m/s for the A_0 mode. In each phase of the experimental procedure, one PZT is selected as the actuator, and the other acts as sensors. All the PZTs act sequentially as actuators. Resulting signals are then simultaneously recorded by the other piezoelectric elements and consist of 1000 data points sampled at 1 MHz.

Table C.2
Mechanical properties of one ply of the chosen composite material.

Density (kg/m^3)	Thickness (mm)	E_{11} (GPa)	E_{22}	E_{33} (GPa)	G_{12} (GPa)	υ_{12}
1554	0.28	60	40	8.1	4.8	0.03

Appendix C. Numerical database for damage localization

To build up the numerical database, a [0°/45°/23°/0°] composite laminate where the mechanical properties of each ply described in Table C.2 is considered. A set of 5 piezoelectric elements (Noliac NCE51), each with a diameter of 20 mm and a thickness of 0.1 mm, are surface-mounted on the composite plate. An illustration of the plate and sensor placement is shown in Fig. 13. Numerical simulations are conducted using SDTools [46]. Squared elements with dimension 2 mm × 2 mm were used for the meshing. The time step for the transient simulation is chosen as 0.3 ms and leads to a sampling frequency of 3.33 MHz. The damage has a circular shape with a 20 mm diameter. The damage is represented by a local reduction in material properties of 90% in the damaged area. Damage cases encompass all combination of damage position with $x = 50, 75, 100, 125, 150, 175, 200$ mm and $y = 125, 130, 135, 140, 145, 150$ mm.

This FEM model was previously validated through experiments [47]. After the simulation, a white Gaussian noise is added to the simulation results for each path between a given actuator and a given sensor in order to simulate experimental noise. Several realizations of this noise constitute an equivalence to the experimental repetitions. A central frequency of $f_0 = 200$ kHz is used with SNR values equal to 150 dB. Here, SNR stands for Signal to Noise Ratio, and the value 0 dB refers to the maximum amount of noise pollution (the energy of the noise being equal to the energy of the signal).

Data availability

Data will be made available on request.

References

[1] Z. Su, L. Ye, Identification of damage using lamb waves, in: Lecture Notes in Applied and Computational Mechanics, vol. 48, Springer London, London, 2009, http://dx.doi.org/10.1007/978-1-84882-784-4.

[2] H. Sohn, C.R. Farrar, F.M. Hemez, J.J. Czarnecki, A review of structural health review of structural health monitoring literature 1996–2001, in: Report Number: la-UR-02-2095, Research Org.: Los Alamos National Lab. (LANL), Los Alamos, NM (United States), 2002.

[3] F.-G. Yuan (Ed.), Structural Health Monitoring (SHM) in Aerospace Structures, in: Woodhead Publishing Series in Composities Science and Engineering, (number 68) Woodhead Publishing is an imprint of Elsevier, Duxford, UK, 2016, OCLC ocn928780081.

[4] A. Deraemaeker, K. Worden, G. Maier, F.G. Rammerstorfer, J. Salençon, B. Schrefler, P. Serafini (Eds.), New Trends in Vibration Based Structural Health Monitoring, in: CISM International Centre for Mechanical Sciences, vol. 520, Springer Vienna, Vienna, 2011, http://dx.doi.org/10.1007/978-3-7091-0399-9.

[5] M. Khanahmadi, M. Gholhaki, O. Rezaifar, B. Dezhkam, Signal processing methodology for detection and localization of damages in columns under the effect of axial load, Measurement 211 (2023) 112595.

[6] M. Khanahmadi, An effective vibration-based feature extraction method for single and multiple damage localization in thin-walled plates using one-dimensional wavelet transform: A numerical and experimental study, Thin-Walled Struct. 204 (2024) 112288.

[7] M. Khanahmadi, B. Mirzaei, G.G. Amiri, M. Gholhaki, O. Rezaifar, Vibration-based damage localization in 3D sandwich panels using an irregularity detection index (IDI) based on signal processing, Measurement 224 (2024) 113902.

[8] K. Worden, C.R. Farrar, G. Manson, G. Park, The fundamental axioms of structural health monitoring, Proc. R. Soc. A: Math. Phys. Eng. Sci. 463 (2082) (2007) 1639–1664, http://dx.doi.org/10.1098/rspa.2007.1834.

[9] Z. Su, L. Ye, Y. Lu, Guided lamb waves for identification of damage in composite structures: A review, J. Sound Vib. 295 (3–5) (2006) 753–780, http://dx.doi.org/10.1016/j.jsv.2006.01.020.

[10] M. Mitra, S. Gopalakrishnan, Guided wave based structural health monitoring: A review, Smart Mater. Struct. 25 (5) (2016) 053001, http://dx.doi.org/10.1088/0964-1726/25/5/053001.

[11] X. Qing, W. Li, Y. Wang, H. Sun, Piezoelectric transducer-based structural health monitoring for aircraft applications, Sensors 19 (3) (2019) 545, http://dx.doi.org/10.3390/s19030545.

[12] C. Zhang, A.A. Mousavi, S.F. Masri, G. Gholipour, The state-of-the-art on time-frequency signal processing techniques for high-resolution representation of nonlinear systems in engineering, Arch. Comput. Methods Eng. (2024) 1–22.

[13] C. Zhang, A.A. Mousavi, S.F. Masri, G. Gholipour, K. Yan, X. Li, Vibration feature extraction using signal processing techniques for structural health monitoring: A review, Mech. Syst. Signal Process. 177 (2022) 109175.

[14] S.G. Mallat, Z. Zhang, Matching pursuits with time-frequency dictionaries, IEEE Trans. Signal Process. 41 (12) (1993) 3397–3415.

[15] B. Xu, V. Giurgiutiu, L. Yu, Lamb waves decomposition and mode identification using matching pursuit method, in: Sensors and Smart Structures Technologies for Civil, Mechanical, and Aerospace Systems 2009, vol. 7292, SPIE, 2009, pp. 161–172.

[16] A. Raghavan, C.E. Cesnik, Guided-wave signal processing using chirplet matching pursuits and mode correlation for structural health monitoring, Smart Mater. Struct. 16 (2) (2007) 355.

[17] D. Chakraborty, N. Kovvali, J. Wei, A. Papandreou-Suppappola, D. Cochran, A. Chattopadhyay, Damage classification structural health monitoring in bolted structures using time-frequency techniques, J. Intell. Mater. Syst. Struct. 20 (11) (2009) 1289–1305.

[18] Y. Lu, J.E. Michaels, Numerical implementation of matching pursuit for the analysis of complex ultrasonic signals, IEEE Trans. Ultrason. Ferroelectr. Freq. Control 55 (1) (2008) 173–182.

[19] W. Mu, Y. Gao, G. Liu, Ultrasound defect localization in shell structures with lamb waves using spare sensor array and orthogonal matching pursuit decomposition, Sensors 21 (23) (2021) 8127.

[20] S. Li, H. Yang, P. Guo, D. Ren, B. Xu, Z. Liang, Damage identification of hinge joint in hollow slab bridge based on model updating and orthogonal matching pursuit algorithm, Measurement 224 (2024) 113867, http://dx.doi.org/10.1016/j.measurement.2023.113867.

[21] Y. Gao, W. Mu, F.-G. Yuan, G. Liu, A defect localization method based on self-sensing and orthogonal matching pursuit, Ultrasonics 128 (2023) 106889, http://dx.doi.org/10.1016/j.ultras.2022.106889.

[22] H. Kim, F.-G. Yuan, Adaptive signal decomposition and dispersion removal based on the matching pursuit algorithm using dispersion-based dictionary for enhancing damage imaging, Ultrasonics 103 (2020) 106087, http://dx.doi.org/10.1016/j.ultras.2020.106087.

[23] H. Li, D. Ai, H. Zhu, H. Luo, An orthogonal matching pursuit based signal compression and reconstruction approach for electromechanical admittance based structural health monitoring, Mech. Syst. Signal Process. 133 (2019) 106276, http://dx.doi.org/10.1016/j.ymssp.2019.106276.

[24] W. Mu, Y. Gao, G. Liu, Ultrasound defect localization in shell structures with lamb waves using spare sensor array and orthogonal matching pursuit decomposition, Sensors 21 (23) (2021) 8127, http://dx.doi.org/10.3390/s21238127.

[25] X. Hong, J. Zhou, Y. He, Damage detection of anchored region on the messenger cable based on matching pursuit algorithm, Mech. Syst. Signal Process. 130 (2019) 221–247, http://dx.doi.org/10.1016/j.ymssp.2019.04.053.

[26] P.W. Tse, X. Wang, Characterization of pipeline defect in guided-waves based inspection through matching pursuit with the optimized dictionary, NDT & E Int. 54 (2013) 171–182, http://dx.doi.org/10.1016/j.ndteint.2012.10.003.

[27] T.D. Bui, K.G. Quach, C.N. Duong, K. Luu, LP norm relaxation approach for large scale data analysis: a review, in: Image Analysis and Recognition: 15th International Conference, ICIAR 2018, Póvoa de Varzim, Portugal, June 27–29, 2018, Proceedings 15, Springer, 2018, pp. 285–292.

[28] Y.S. Soh, Group invariant dictionary learning, IEEE Trans. Signal Process. 69 (2021) 3612–3626.

[29] T.Y. Hou, Z. Shi, Sparse time-frequency decomposition by dictionary learning, 2013, arXiv preprint arXiv:1311.1163.

[30] J. Hua, L. Zeng, F. Gao, J. Lin, Dictionary design for lamb wave sparse decomposition, NDT & E Int. 103 (2019) 98–110.

[31] S. Cuomo, M. Boccaccio, M. Meo, Damage identification during an impact event using the Hilbert-Huang transform of decomposed propagation modes, Mech. Syst. Signal Process. 191 (2023) 110126.

[32] Y. Jiang, S. Chen, K. Wang, W. Liao, H. Wang, Q. Zhang, Quantitative detection of rail head internal hole defects based on laser ultrasonic bulk wave and optimized variational mode decomposition algorithm, Measurement 218 (2023) 113185.

[33] R. Zeng, Q. Wu, L. Zhang, Two-terminal traveling wave fault location based on successive variational mode decomposition and frequency-dependent propagation velocity, Electr. Power Syst. Res. 213 (2022) 108768.

[34] V. Serov, et al., Fourier Series, Fourier Transform and Their Applications to Mathematical Physics, vol. 197, Springer, 2017.

[35] J.L. Troutman, Variational Calculus and Optimal Control: Optimization with Elementary Convexity, Springer Science & Business Media, 2012.

[36] S.J. Orfanidis, Electromagnetic Waves and Antennas, Rutgers University New Brunswick, NJ, 2002.

[37] L. Cohen, Pulse propagation in dispersive media, in: Proceedings of the Tenth IEEE Workshop on Statistical Signal and Array Processing (Cat. No. 00TH8496), IEEE, 2000, pp. 485–489.

[38] M. Rébillat, O. Hmad, F. Kadri, N. Mechbal, Peaks over threshold–based detector design for structural health monitoring: Application to aerospace structures, Struct. Health Monit. 17 (1) (2018) 91–107.

[39] M. Rébillat, N. Mechbal, Damage localization in geometrically complex aeronautic structures using canonical polyadic decomposition of Lamb wave difference signal tensors, Struct. Health Monit. 19 (1) (2020) 305–321.

[40] S. Guo, M. Rébillat, N. Mechbal, Prediction of frequency and spatially dependent attenuation of guided waves propagating in mounted and unmounted A380 parts made up of anisotropic viscoelastic composite laminates, Struct. Health Monit. (2022).

[41] M. Ducousso, F. Reverdy, Real-time imaging of microcracks on metallic surface using total focusing method and plane wave imaging with Rayleigh waves, NDT & E Int. 116 (2020) 102311.

[42] M. Tanter, M. Fink, Ultrafast imaging in biomedical ultrasound, IEEE Trans. Ultrason. Ferroelectr. Freq. Control 61 (1) (2014) 102–119.

[43] A. Fitzpatrick, A. Singhvi, A. Arbabian, An airborne sonar system for underwater remote sensing and imaging, IEEE Access 8 (2020) 189945–189959.

[44] D. Poirier-Quinot, B.F. Katz, M. Noisternig, EVERTims: Open source framework for real-time auralization in architectural acoustics and virtual reality, in: 20th International Conference on Digital Audio Effects, DAFx-17, 2017.

[45] N. Eley, S. Mullins, P. Stitt, B.F. Katz, Virtual notre-dame: Preliminary results of real-time auralization with choir members, in: 2021 Immersive 3D Audio: From Archit. Automot. (I3DA), I3DA, IEEE, 2021, pp. 1–6.

[46] E. Balmes, Structural dynamics toolbox (for use with MATLAB), 2020, www.sdtools.com.

[47] C. Fendzi, N. Mechbal, M. Rébillat, M. Guskov, G. Coffignal, A general Bayesian framework for ellipse-based and hyperbola-based damage localization in anisotropic composite plates, J. Intell. Mater. Syst. Struct. 27 (3) (2016) 350–374, http://dx.doi.org/10.1177/1045389X15571383.